Behavioral/Systems/Cognitive

Recurrent Connection Patterns of Corticostriatal Pyramidal Cells in Frontal Cortex

Mieko Morishima and Yasuo Kawaguchi
Division of Cerebral Circuitry, National Institute for Physiological Sciences, Department of Physiological Sciences, The Graduate University for Advanced Studies, Aichi, Okazaki 444-8787, Japan

Corticostriatal pyramidal cells are heterogeneous in the frontal cortex. Here, we show that subpopulations of corticostriatal neurons in the rat frontal cortex are selectively connected with each other based on their subcortical targets. Using paired recordings of retrogradely labeled cells, we investigated the synaptic connectivity between two projection cell types: those projecting to the pons [corticopontine (CPn) cell], often with collaterals to the striatum, and those projecting to both sides of the striatum but not to the pons [crossed corticostriatal (CCS) cell]. The two types were morphologically differentiated in regard to their apical tufts. The dendritic morphologies of CCS cells were correlated with their somatic depth within the cortex. CCS cells had reciprocal synaptic connections with each other and also provided synaptic input to CPn cells. However, connections from CPn to CCS cells were rarely found, even in pairs showing CCS to CPn connectivity. Additionally, CCS cells preferentially innervated the basal dendrites of other CCS cells but made contacts onto both the basal and apical dendrites of CPn cells. The amplitude of synaptic responses was to some extent correlated with the contact site number. Ratios of the EPSC amplitude to the contact number tended to be larger in the CCS to CCS connection. Therefore, our data demonstrate that these two types of corticostriatal cells distinct in their dendritic morphologies show directional and domain-dependent preferences in their synaptic connectivity.

Key words: **pyramidal cell; frontal cortex; striatum; pons; postsynaptic current; apical dendrite**

Introduction

In the neocortex, pyramidal cells projecting to the same target areas are aggregated within given cortical layers, with each layer containing several projection types (Jones, 1984; Kasper et al., 1994; Gao and Zheng, 2004). Even within microregions of the same cortical layer, there can exist several projection cell types (Lévesque et al., 1996b; Vercelli et al., 2004; Gabbott et al., 2005). Pyramidal cells are recurrently connected with each other (Markram, 1997; Markram et al., 1997; Thomson and Deuchars, 1997; Gao et al., 2001), and recurrent excitatory interactions in groups of neurons induce slow rhythmic depolarizations (depolarized "up" states) during sleep or anesthesia (Metherate and Ashe, 1993; Steriade et al., 1993; Stern et al., 1997). Additionally, reverberating excitation by recurrent connections may be important for information processing in cortical circuits (Anderson et al., 2000; Wang, 2001). Considering the interlaminar connectivity of pyramidal cells, the reverberating excitation could occur in individual cortical layers (Thomson and Morris, 2002), perhaps within layer V (Sanchez-Vives and McCormick, 2000). Although the specific synaptic connectivity of cortical projection neurons within the same layer is not yet established, recent data suggest that different classes of cortical neurons within a layer may show selective connectivity (Mercer et al., 2005), a finding that has important implications for our understanding of the function of the cortex.

In the frontal cortex, two classes of corticostriatal pyramidal cells have been identified in layer V based on their axonal projection patterns (Cowan and Wilson, 1994). Crossed corticostriatal (CCS) cells innervate both the ipsilateral and contralateral striatum, whereas other corticostriatal cells selectively innervate the ipsilateral striatum but project also to the brainstem through the pyramidal tract. Some brainstem projecting neurons include cells projecting to the pontine nuclei [corticopontine (CPn) cells]. In the rat frontal cortex, brainstem-projecting layer V neurons also frequently innervate the ipsilateral striatum (Cowan and Wilson, 1994; Lévesque et al., 1996a; Lévesque and Parent, 1998). These corticostriatal pyramidal cells transmit the slow oscillation generated within the frontal cortex to striatal cells (Wilson and Groves, 1981; Wilson and Kawaguchi, 1996; Stern et al., 1998). It remains to be determined how the oscillation is produced in the individual cortical layers and propagated to the striatal neurons (Stern et al., 1997).

Because different classes of corticostriatal cells innervate distinct populations of striatal cells (Lei et al., 2004) that have opposing effects on the outputs of basal ganglia (Albin et al., 1989; Alexander and Crutcher, 1990), knowledge of the patterns of synaptic connectivity between corticostriatal cells may suggest a physiological substrate for cortical influence on the basal ganglia

Received Jan. 19, 2006; revised March 11, 2006; accepted March 14, 2006.

This work was supported by grants-in-aid for scientific research from the Ministry of Education, Culture, Sports, Science and Technology of Japan. M.M. is a research fellow of the Japan Society for the Promotion of Science. We thank Drs. F. Karube, S. Kondo, and Y. Kubota for helpful discussions; M. Saito for technical assistance; and Drs. A. Gulledge and A. Agmon for comments on this manuscript.

Correspondence should be sent to Yasuo Kawaguchi, Division of Cerebral Circuitry, National Institute for Physiological Sciences, Myodaiji, Okazaki 444-8787, Japan. E-mail: yasuo@nips.ac.jp.

DOI:10.1523/JNEUROSCI.0252-06.2006

 0270-6474/06/264394-12$15.00/0

circuitry. To this end, we investigated the synaptic connections between retrograde-labeled CCS and CPn pyramidal cells. Our results demonstrate distinct morphologies and selective patterns of synaptic connectivity between CCS and CPn cells.

Materials and Methods

Dual fluorescent retrograde labeling of CCS and CPn cells. Retrograde labeling experiments were performed on young [postnatal day 19 (P19) to P23] Wistar rats. Rats were anesthetized with ketamine (40 mg/kg, i.m.) and xylazine (4 mg/kg, i.m.). Two different fluorescent retrograde tracers were applied by pressure injection (PV820; WPI, Sarasota, FL) into the pons and striatum, respectively, of each animal using glass pipettes (tip diameter, 100 μm) (see Fig. 1*A*). In the case of striatal injection, the cortex, hippocampus, and fimbria just caudal to the striatum were removed by suction, and the tracer was applied obliquely through the lateral ventricle to prevent tracer spilling into the cortex. Alexa Fluor 555-conjugated cholera toxin subunit B (CTB; Invitrogen, San Diego, CA) was injected into the striatum contralateral to the cortex investigated (80–100 nl, 0.8 mm posterior to bregma, 2.5 mm lateral to bregma; depth, 4 mm) (see Fig. 1*A1*). Fast Blue (7% in distilled water; Illing Plastics, Breuberg, Germany) or Fluorogold (4% in distilled water; Fluorochrome, Englewood, NJ) was injected into the pons including the ipsilateral pontine nuclei (80–100 nl, 5.6 mm posterior to bregma, 0.5–1 mm lateral to bregma; depth, 9–9.5 mm) (see Fig. 1*A2*). After a survival period of 4 d, the animals were anesthetized with sodium pentobarbital (60 mg/kg, i.p.) and perfused transcardially with saline followed by a fixative containing 4% paraformaldehyde and 0.2% picric acid in 0.1 M sodium phosphate buffer (PB). The frontal cortex was obliquely sectioned at 20 μm on a cryostat (Kawaguchi, 1992), and sections were mounted on glass slides and coverslipped in Krystalon mounting medium (EM Science, Fort Washington, PA). The sections were observed by epifluorescence (excitation, 360–370 nm; emission, 420- for Fast Blue or Fluorogold; excitation, 545–580 nm; emission, 610- for Alexa Fluor 555-CTB).

For physiological experiments using an *in vitro* slice preparation (see below), rhodamine-labeled latex microspheres (RLMs) (80–100 nl; Lumafluor, Naples, FL) were injected into the contralateral striatum, and CTB (80–100 nl) into pontine nuclei 2–3 d before the experiment (see Fig. 1*A*). Pyramidal cells labeled with RLMs could be discriminated from those with CTB, because the former showed a granular staining pattern, whereas the latter were homogeneously stained in the cytosol (see Fig. 2*A*).

Slice preparation. Animals were deeply anesthetized with isoflurane and decapitated. Brains were quickly removed and submerged into ice-cold physiological Ringer's solution. Three hundred-micrometer-thick sections of frontal cortex (medial agranular and anterior cingulate cortex) were cut and immersed in a buffered solution containing the following (in mM): 124 NaCl, 3 KCl, 2.4 $CaCl_2$, 1.2 $MgCl_2$, 26 $NaHCO_3$, 1 NaH_2PO_4, 10 glucose, 4 lactic acid, 0.2 ascorbic acid. This solution was continuously aerated with a mixture of 95% O_2 and 5% CO_2. During recording, lactic acid was omitted. Membrane potentials of retrogradely labeled cells in the frontal cortex (medial agranular cortex and anterior cingulate cortex) were recorded in a whole-cell mode at 29°C. Retrogradely labeled cells were identified by epifluorescence (excitation, 520–550 nm; emission, 580), under a 40× water immersion objective.

Electrophysiological recording. The pipette solution for current-clamp recording consisted of the following (in mM): 126 potassium methylsulfate, 6 KCl, 0.6 EGTA, 2 $MgCl_2$, 4 ATP, 0.3 GTP, 10 HEPES, and 0.75% biocytin (Sigma, St. Louis, MO). The pH of the solution was adjusted to 7.3 with KOH, and the osmolarity was ~290 mOsm. Current-clamp recordings were made in a fast current-clamp mode of EPC9/dual (HEKA Elektronik , Lambrecht/Pfalz, Germany).

EPSC analysis. EPSCs were induced by single presynaptic action potentials generated by depolarizing somatic current pulses (duration, 10 ms) in the presynaptic cells and were measured in postsynaptic neurons voltage clamped at −60 mV at a sampling rate of 20 kHz. Series resistance of the postsynaptic whole-cell recordings was monitored periodically by the delivery of small voltage pulses (−5 mV, 10 ms) to the postsynaptic neuron. Recordings were ended when spikes in the presynaptic cell deteriorated or if the series resistance in the postsynaptic cell increased. Postsynaptic responses to single action potentials were identified from individual current traces and averaged over at least 20 trials. Electrophysiological data were analyzed by IGOR Pro (WaveMetrics, Lake Oswego, OR). To obtain the peak current of each trace, the current amplitudes (time window, 0.2 ms; five points) were averaged around the EPSC maximum after excluding failure current traces. The baseline current was defined as the averaged current in a window (2 ms duration) before application of depolarizing current pulses to the presynaptic cell. The peak EPSC is the peak current minus the baseline. Spontaneous synaptic currents were analyzed by Mini Analysis (Synaptosoft, Decatur, GA).

The EPSC rise time was calculated from 20 to 80% of the peak EPSC amplitude. The onset was defined as the point at which a line extrapolated from the rise time crossed the baseline current. Latency was measured from the peak of the presynaptic spike to the EPSC onset. The decay time constant was obtained by fitting a single exponential. To average EPSC traces, the peaks of presynaptic spikes were aligned. EPSC frequency characteristics at 10 Hz were obtained from pairs having EPSCs with mean amplitudes larger than 6 pA. The coefficient of variation (CV) was obtained in the pairs with >40 EPSCs.

Histology. Tissue slices containing biocytin-loaded cells were fixed by immersion in 4% paraformaldehyde, 1.25% glutaraldehyde, and 0.2% picric acid overnight at 4°C, and followed by a freeze-thawing procedure in sucrose-containing PB using liquid nitrogen twice. Slices were resectioned at a thickness of 50 μm. Sections were incubated with avidin–biotin–peroxidase complex (1:100; Vector Laboratories, Burlingame, CA) in 0.05 M Tris-HCl-buffered saline (TBS) with 0.04% Triton X-100 overnight at 4°C. After washing in TBS, the slices were reacted with 3,3′-diaminobenzidine tetrahydrochloride (0.02%), nickel ammonium sulfate (0.3%), and H_2O_2 (0.003%) in Tris-HCl buffer. They were then postfixed in

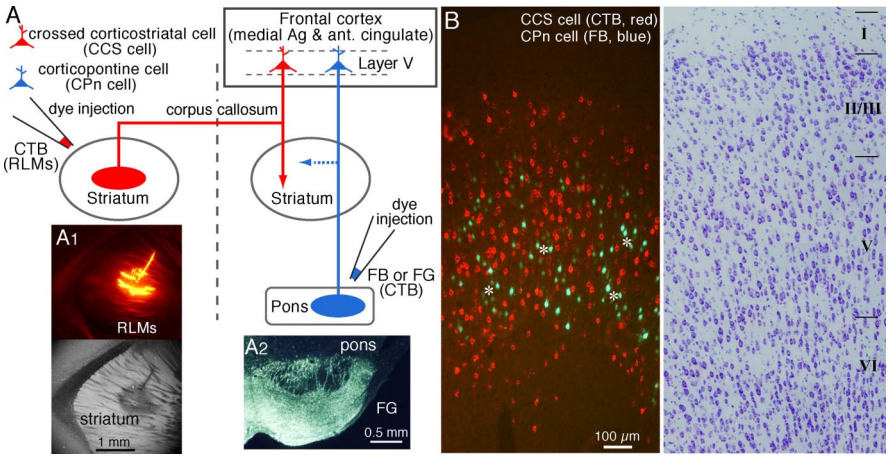

Figure 1. Two projection types of pyramidal cells in layer V of the frontal cortex. ***A***, Schematic of method for identification of two projection neuron types by retrograde tracers. Alexa Fluor 555-conjugated CTB was injected in the contralateral striatum while Fast Blue (FB) or Fluorogold (FG) was injected into the pontine nuclei. For simultaneous recording from CCS and CPn cells, RLMs were injected in the contralateral striatum, and CTB was injected in the ipsilateral pons. Ag, Agranular; ant., anterior. ***A1***, Injection site of RLMs in the striatum. Top, Epifluorescence view. Bottom, As in above, but using bright-field microscopy. The tracer was applied obliquely through the lateral ventricle after suctioning the overlying cortex to prevent injection into the cortex. ***A2***, Injection site of Fluorogold in the pons including the ipsilateral pontine nuclei. ***B***, Fluorescence imaging revealed two nonoverlapping populations of CCS and CPn cells. CPn cells were distributed in patchy regions (asterisks) where CCS cells were absent. Right, As in the left but in thionin staining.

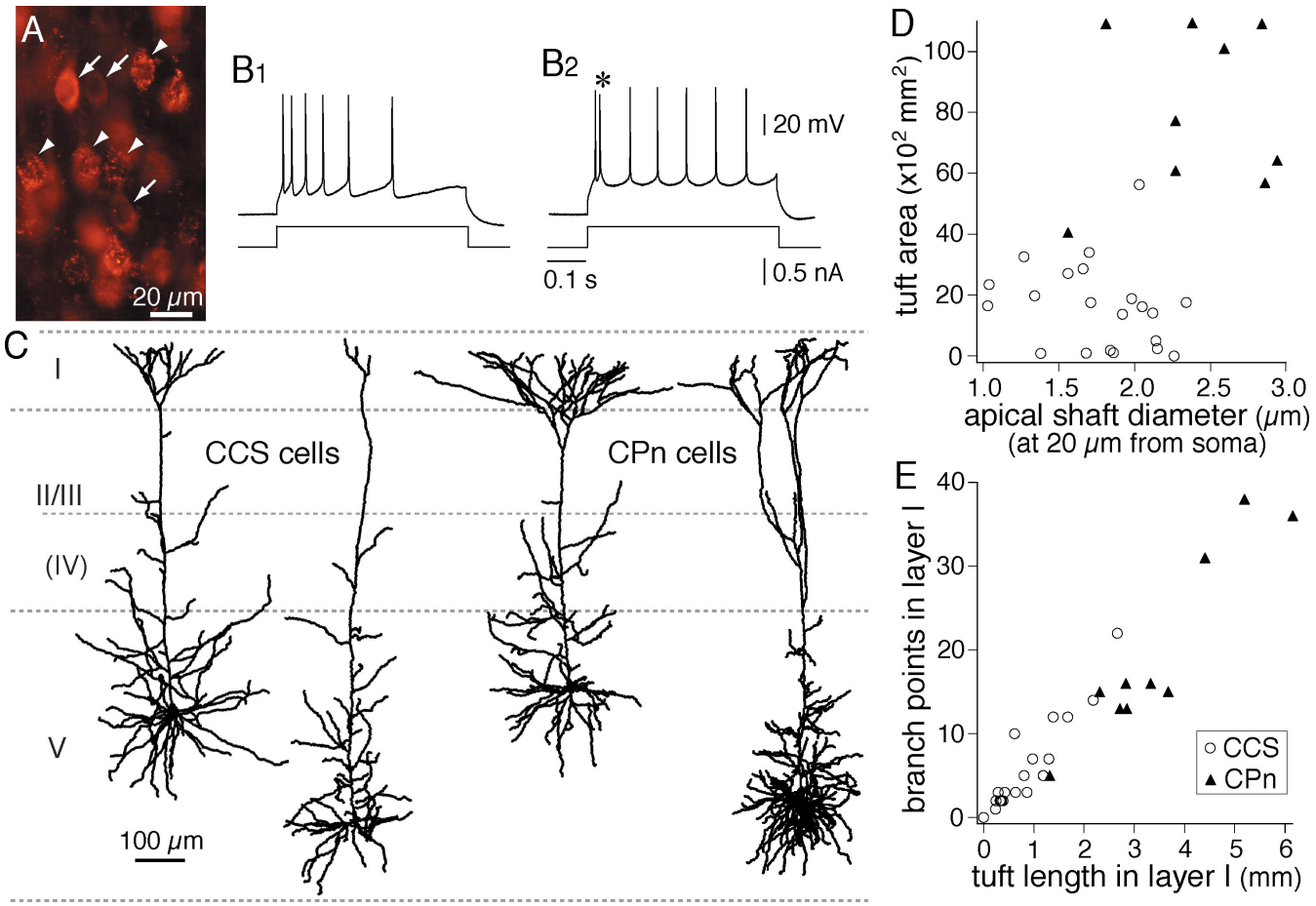

Figure 2. Morphological characteristics of the two projection types of pyramidal cells. ***A***, Simultaneous fluorescent labeling of CCS cells with RLMs (arrowheads) and CPn cells with CTB (arrows). ***B1***, ***B2***, Firing responses of CCS and CPn cells, respectively. Note the initial doublet firing (*) in a CPn cell. ***C***, Dendritic reconstructions of two CCS and two CPn cells, showing the differences in dendritic patterns, especially in their apical tufts. ***D***, Plot of the differences in the apical tuft area and shaft diameter between CCS (open circles) and CPn (filled triangles) cells. ***E***, Differences in the dendritic length of layer I tufts and branch points in layer I between CCS and CPn cells.

1% OsO_4 in PB containing 7% glucose, dehydrated, and flat-embedded on silicon-coated glass slides in Epon. After all of the procedures, the tissue shrank to ~90% in length (Karube et al., 2004). The shrinkage was not corrected in the analysis.

Quantitative morphology. Somata, axons, and dendrites of stained cells were reconstructed three-dimensionally using the Neurolucida system (MicroBrightField, Williston, VT). Stained cells were drawn for reconstruction with a 60× or 100× objective combined with an additional 1.25× magnification. The apical shaft diameter was obtained by the cross-sectional area of the straight portion ~20 μm far from the somatic origin divided by the measured dendritic length. Reconstructed axons and dendrites were composed of serial points with intervals shorter than 1.5 μm (see Fig. 8, inset). Reconstructed neurons were quantitatively analyzed with NeuroExplorer (MicroBrightField, Colchester, VT). Internode intervals are lengths between two successive nodes (branch points) along the dendrite, including those from the soma origin to the first node. Internode tortuosity is the ratio of the internode interval to the direct distance between nodes. The basal field and tuft area were areas

Table 1. Somatic and dendritic comparisons of CCS and CPn cells in layer V

	CCS	CPn
Somata	($n = 24$)	($n = 10$)
Volume (μm^3)	5150 ± 1642	5718 ± 1507
Basal dendrites	($n = 25$)	($n = 9$)
Primary dendrite number	7.8 ± 1.3	9 ± 2.3
Nodes (branching points)	24.3 ± 5.9	34.6 ± 13**
Internode interval (mean, μm)	22.8 ± 5.3	24.8 ± 5
Internode tortuosity	1.14 ± 0.08	1.2 ± 0.1
Area (× 100 μm^2)	731 ± 293	650 ± 200
Endings[a]		
Order (mean)	3.6 ± 0.5	3.8 ± 0.4
Horizontal direct distances (mean, μm)	110 ± 18	99 ± 15
Vertical direct distances (mean, μm)	77 ± 17	63 ± 10**
Apical dendrites	($n = 24$)	($n = 8$)
Apical origin (distance from pia, μm)	825 ± 200	760 ± 103
Shaft diameter (at 20 μM from soma, μm)	1.79 ± 0.37	2.34 ± 0.48**
Oblique branch density (/100 μm)	2.3 ± 0.5	2.8 ± 0.8
Apical tufts	($n = 26$)	($n = 10$)
Layer I dendritic length (μm)	878 ± 684	3478 ± 1431**
Layer I branch points	6.0 ± 5.3	19.8 ± 11.1**
Tuft area (× 100 μm^2)	215 ± 129[c]	876 ± 330**
Tuft origin (vertical position from pia,[b] μm)	208 ± 66[c]	350 ± 110**

Data are means ± SD. *n*, Number of cells. **$p < 0.01$.

[a]True endings.

[b]White matter side, positive.

[c]CCS cells with the tuft structure ($n = 20$).

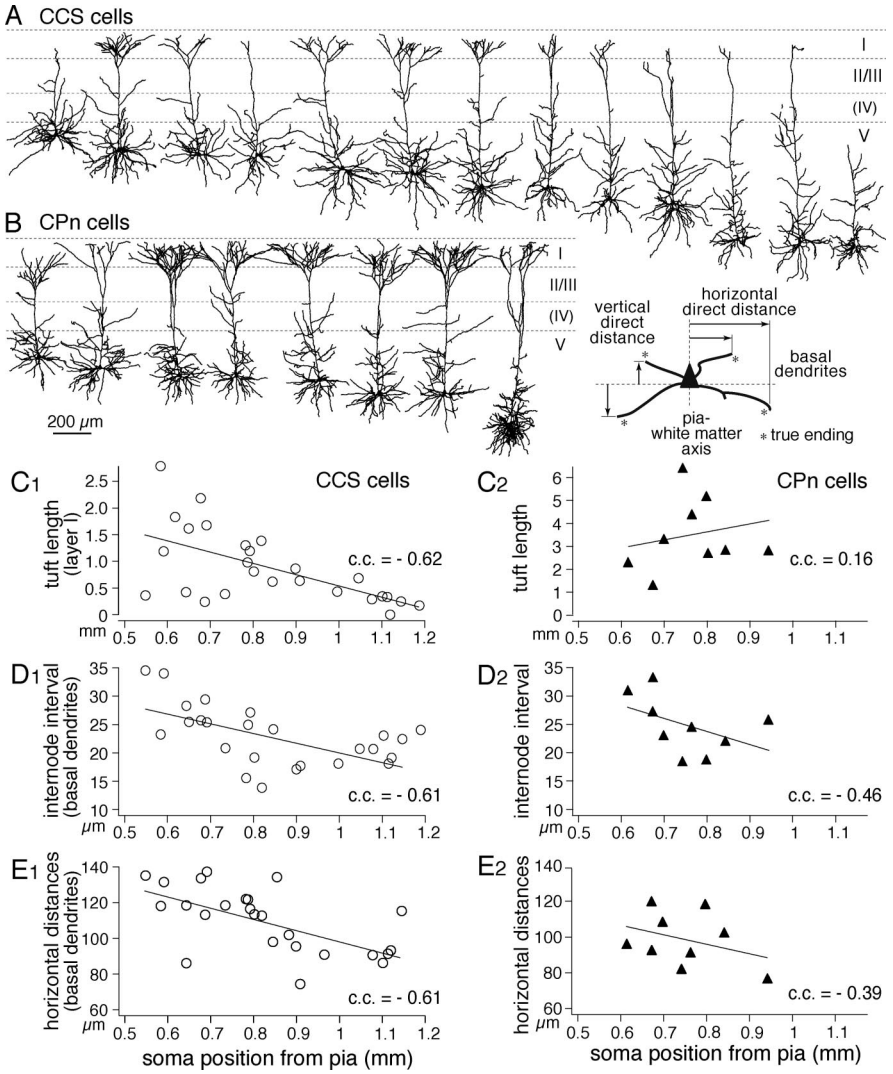

Figure 3. Depth dependency of dendritic morphologies among CCS cells. ***A***, ***B***, Dendritic reconstructions of CCS cells (top) and CPn cells (bottom), arranged from most superficial to deeper somata in layer V. ***C–E***, Depth profiles of dendritic lengths in layer I (***C***), mean internode intervals of basal dendrites (***D***), and horizontal direct distances of basal dendrite endings (***E***) (inset defines the parameters of endings). Note the depth dependency of these parameters in CCS cells. Lines are linear fits.

of the plane perpendicular to the pia-white matter axis, onto which the basal dendrites and apical tufts were projected, respectively. To evaluate the dendritic extension, we measured direct distances between the soma centroid and true endings, not endings resulting from slice preparation, along horizontal and vertical axes (horizontal and vertical distances, respectively) (see Fig. 3*B*, inset).

Potential synaptic contacts (contact sites) were identified as a close apposition of an axonal bouton and a postsynaptic dendrite in the same focal plane at 1250× using a 100× objective (numerical aperture, 1.4) (Markram et al., 1997; Feldmeyer et al., 1999). When the presynaptic axons and postsynaptic dendrites came close within 2.5 μm between the centers of neurites, the nearest encounter sites of dendrites were called approach points (approaches) (see Fig. 8, inset). Data are given as mean ± SD. For statistical comparison of the mean measurements between two cell classes, the Mann–Whitney *U* test was used.

Results

Morphological differences between CCS and CPn cells

To confirm that CCS and CPn cells were distinct cell types, we used two different fluorescent tracers injected into their projection target areas (three rats). CTB was injected into the contralateral striatum ($n = 3$), and Fast Blue ($n = 2$) or Fluorogold ($n = 1$) was injected into the pons, including the ipsilateral pontine nuclei (Fig. 1*A*). Sections of the medial agranular and anterior cingulated cortex were subsequently processed and visualized with epifluorescence. The labeled cells of both types were found mostly in layer V, but CCS cells were sometimes in the lower part of layer II/III (Fig. 1*B*) To count fluorescent cells, we selected regions where both fluorescences overlapped strongly. We found 2298 fluorescently labeled cells from three rats. Of these, 1141 were labeled with CTB (CCS cells), and 1157 were labeled with Fast Blue or Fluorogold (CPn cells). Importantly, double-labeled cells were never observed, indicating that two types belonged to completely separate neuronal populations. In addition, CPn cells were distributed in patchy regions where CCS cells were absent (Fig. 1*B*). The two types of pyramidal cells seemed to occupy complementary spaces in layer V.

In layer V, we recorded from CPn cells labeled with Alexa 555 CTB injected into the pons, including the ipsilateral pontine nuclei (Wang and McCormick, 1993) and CCS cells labeled with RLMs injected into the contralateral striatum (Fig. 1*A*). Red dyes were used for recording because of less damage to the cells during fluorescence observation. Cells labeled by these red tracers could be differentiated, because RLMs generate granular staining, whereas CTB produces homogeneous fluorescence except within nuclei (Fig. 2*A*). Resting potentials were −66.4 ± 5.4 mV in CCS cells ($n = 20$) and −62.1 ± 4.1 mV in CPn cells ($n = 10$), and input resistances were 139.3 ± 60.1 MΩ in CCS and 90.6 ± 82.5 MΩ in CPn cells. Among 11 CPn cells, nine cells showed initial doublet spikes and in response to step depolarization (Fig. 2*B2*), followed by nonadaptive repetitive firing (Mason and Larkman, 1990; Hefti and Smith, 2000; Christophe et al., 2005). In contrast, CCS cells ($n = 28$) displayed no initial doublet firing to step depolarizations (Fig. 2*B1*).

We compared the dendritic and axonal patterns of biocytin-filled CCS and CPn cells. In the basal dendrites, the primary dendrite number and internode interval were similar between the two types (Table 1). The apical dendrites of the two neuronal types showed similar branch density along the shaft, but CPn cells had significantly thicker shaft diameters at their base than did CCS cells (measured at ~20 μm from the somatic origin; $p < 0.01$) (Fig. 2*D*, Table 1). Additionally, the apical tufts of the two types of neuron were morphologically distinct (Fig. 2*C–E*, Table 1). CPn cells had larger tuft areas, longer lengths of layer I dendrites, and more branch points in layer I than did CCS cells ($p < 0.01$). Additionally, the tufts of CPn cells originated from the main apical shafts at a greater depth than in CCS cells (Table 1) ($p < 0.01$). Both types had axon collaterals around the somata and included cells innervating layer I (data not shown). Horizontal collaterals were observed in both types, but CPn cells seemed

to extend further than CCS cells. Together, these data demonstrate that CCS and CPn cells are morphologically differentiated in regard to their apical tufts. However, significant heterogeneity was observed among the apical tufts of both CPn and CCS cells (Fig. 2*D*,*E*).

Depth dependence of dendritic patterns in CCS cells

We next asked whether the morphological diversity observed in CCS and CPn cells might depend on their somatic locations within layer V. To test for this, we aligned dendritic reconstructions of CCS and CPn cells in accordance with somatic depth from the pia (Fig. 3*A*,*B*). The dendritic morphologies of CCS cells changed gradually according to their depth within layer V. Some superficial CCS cells had robust apical tufts (tufted CCS cells), whereas others had poorly developed tufts (slender CCS cells). The apical dendrites of deeper CCS cells tended to have a very reduced or absent apical tuft resembling the superficial slender CCS cells. Tuft dendritic lengths in layer I were heterogeneous in neurons with superficial somata but were significantly shorter in neurons with somata in the deeper areas of layer V (Fig. 3*C1*) ($p < 0.01$). Additionally, the internode intervals in the basal dendrites were longer in superficial CCS cells and shorter in deeper CCS cells (Fig. 3*D1*) ($p < 0.01$). To compare the dendritic spatial spread, we measured horizontal direct distances between soma centroid and true endings. Horizontal dendritic distances were longer in superficial CCS cells (Fig. 3*E1*) ($p < 0.01$). Correspondingly, the basal dendritic fields of superficial layer V CCS cells were larger than those of deeper CCS cells [correlation coefficient (c.c.), −0.58; $p < 0.01$]. These depth-dependent tendencies were absent or much less pronounced in CPn cells (Fig. 3*C2–E2*) (tuft lengths, $p = 0.7$; internode intervals, $p = 0.22$; in horizontal distances, $p = 0.31$; c.c., −0.24 in basal dendritic field; $p = 0.55$). Total dendritic length was negatively correlated with the distance between the pia and soma in CCS cells (c.c., −0.44; $p < 0.05$) but positively in CPn cells (c.c., 0.85; $p < 0.01$) because of the length increase of apical shaft and their branches in deeper CPn cells. These data demonstrate that although CCS cells are heterogeneous in their dendritic structures, there is a significant correlation between the size and robustness of their dendritic fields and their sublaminar position within layer V.

EPSC characteristics and connection patterns

To reveal synaptic connection patterns between CCS and CPn cells, we investigated the EPSC characteristics and connection probability using paired recordings consisting of a CCS cell and another CCS or CPn cell in layer V (Fig. 4*A*). EPSCs were induced with connection probability of 0.1 in pairs from CCS to CCS ($n = 308$) and 0.11 in CCS to CPn pairs ($n = 98$) within 100 μm in distance but were rarely found from CPn to CCS cells. It was only found once in 96 pairs (Fig. 4*B*). Among 31 connections from CCS to CCS cells, four were reciprocal (connection probability, 0.13). EPSC characteristics were examined in cell pairs in which series resistances of postsynaptic recordings were low. EPSC latencies and amplitudes were similar between CCS to CCS ($n = 24$) and CCS to CPn pairs ($n = 11$) ($p = 0.17$ and 0.94, respectively) (Table 2). The EPSC rise time and decay time constants were also similar ($p = 0.12$ and 0.78, respectively) (Table 2). Spontaneous EPSCs were also similar in amplitudes between CCS and CPn cells [10.5 ± 1.8 pA in CCS cells ($n = 6$) and 10.9 ± 2.8 pA in CPn cells ($n = 6$)] but more variable in CPn cells (CV, 0.4 ± 0.08 in CCS and 0.82 ± 0.55 in CPn cells). Mean amplitudes of evoked unitary EPSCs did not correlate with those of spontaneous EPSCs (c.c., −0.05; $p = 0.88$; $n = 12$), suggesting unitary EPSC amplitudes were not affected by the postsynaptic cell condition. To examine short-term synaptic dynamics in these connections, pairs of EPSCs were generated at 100 ms intervals. The paired-pulse ratios of the second EPSC to first EPSC were smaller in CCS cells ($n = 15$) than in CPn cells ($n = 4$) (Table 2) but not significantly different ($p = 0.07$). These data show that CCS cells are connected with other CCS cells and with CPn cells, but CPn cells are rarely connected with CCS cells. Additionally, the postsynaptic currents generated by presynaptic CCS cells were quantitatively similar regardless of their postsynaptic target.

The distances between the somata of connected CCS to CCS

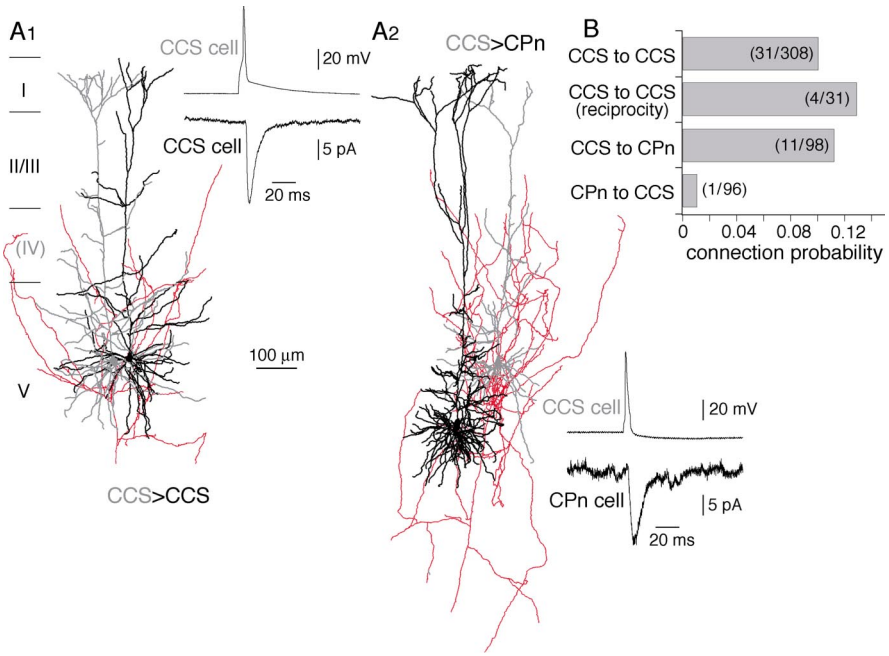

Figure 4. Synaptic connections among corticostriatal pyramidal cells. ***A1***, Reconstructions of the dendrites of presynaptic (gray) and postsynaptic (black) CCS cells and the axon of the presynaptic CCS cell (red). Inset, A presynaptic action potential (top trace) generates a unitary postsynaptic current (bottom trace). ***A2***, Reconstructions and postsynaptic current of a presynaptic CCS cell (gray) and postsynaptic CPn (black) cells. ***B***, Connection probability between pyramidal cell subtypes. Note that very few connections were found from CPn to CCS cells.

Table 2. Unitary EPSC characteristics in CCS and CPn cells, induced by CCS cells

	CCS ($n = 24$)	CPn ($n = 11$)
Latency (ms)	1.6 ± 0.6	1.8 ± 0.5
Amplitude (pA)	17.8 ± 15.4	14.7 ± 9.6
Rise time (ms)	0.9 ± 0.4	1.1 ± 0.5
Decay time constant (ms)	6.0 ± 2.0	6.3 ± 2.5
Paired-pulse ratio (second/first; 10 Hz)	0.77 ± 0.26[a]	0.93 ± 0.12[b]

Data are means ± SD. *n*, Number of cells.

[a] $n = 15$.

[b] $n = 4$.

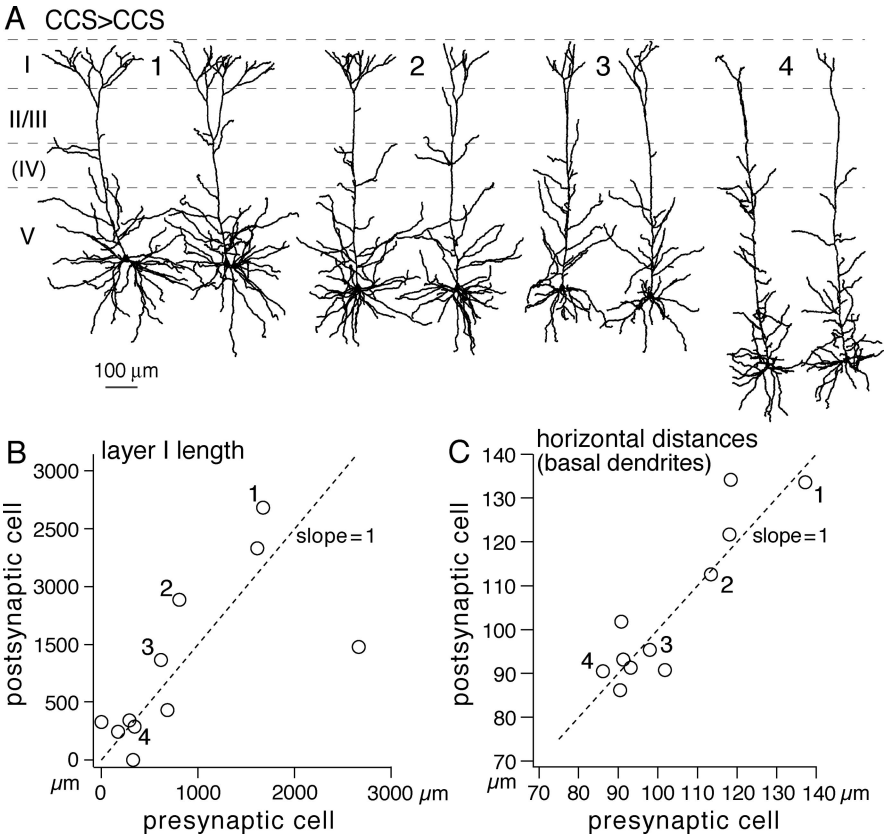

Figure 5. Synaptically connected CCS cells show similar dendritic morphologies. ***A***, Dendritic reconstructions of four connected CCS cell pairs (1–4). The left is presynaptic cells. In pair 4, the cells were bidirectionally connected. Spatially overlapped neurons in the pairs are separate to see individual morphologies. Note the comparable dendritic patterns between CCS cell pairs. ***B***, Comparison of dendritic lengths in layer I between presynaptic and postsynaptic cells. ***C***, Comparison of mean horizontal direct distances of endings (Fig. 3, inset). Note the presynaptic and postsynaptic dendritic similarity. Numbers (1–4) in ***B*** and ***C*** correspond to those of pairs in ***A***.

pairs reconstructed were 63 ± 42 μm (22 ± 16 μm in horizontal direction and 54 ± 46 μm in vertical one; $n = 19$). Those of connected CCS to CPn pairs were 84 ± 53 μm ($p = 0.39$; 25 ± 25 μm in horizontal direction and 76 ± 53 μm in vertical one; $n = 9$). These values are consistent with previous data showing that the highest density of connected pyramidal cells is found within 25 μm in the horizontal direction and 50 μm in the vertical one, and that the connection probability and EPSP amplitude are greatly reduced when the distance between pairs is larger than 100 μm (Holmgren et al., 2003).

Because CCS cells at the same depth within layer V tended to have similar dendritic patterns (Fig. 3), and most connections were found between neurons with somata within 100 μm of each other, connected CCS cells tended to have similar dendritic morphologies (Fig. 5*A*). No such correlation was found between the dendritic morphologies of synaptically connected CCS and CPn pairs. The dendritic lengths of tuft branches in layer I were found to be similar in connected CCS pairs (Fig. 5*B*) (c.c., 0.68; $p < 0.05$; slope against the presynaptic cell, 0.6), as were their basal dendritic structures. The mean internode intervals of basal dendrites were similar in CCS pairs that were synaptically connected (c.c., 0.46; $p = 0.16$; slope, 0.71). The connected CCS pairs correlated in horizontal distances (Fig. 5*C*) (c.c., 0.91; $p < 0.01$; slope, 1.01) and in vertical distances (c.c., 0.74; $p < 0.01$; slope, 1.12). The area of basal dendritic field was also correlated in connected CCS pairs (c.c., 0.84; $p < 0.01$; slope, 0.82). Because the somata of recorded pairs were typically within 100 μm of each other, it is likely that the depth dependence of dendritic morphology contributes to the morphological resemblance of synaptically connected CCS cell pairs.

Contact site distributions between connected pairs and their relation to EPSC amplitudes

To test whether target-specific differences exist in synapse formation onto postsynaptic CCS or CPn cells, we reconstructed the axons and dendrites of paired neurons (Fig. 6*A1*,*A2*). Contact points between boutons and postsynaptic dendrites were mapped on dendrograms (Fig. 6*A1–A3*), and their distances from somata were compared (Fig. 6*B*). Contact sites in both types of pairs were found on dendritic branches within layer V. No significant differences were found when comparing the mean distances of contact sites from the soma (Table 3) or the dendritic order of contact sites (Table 3). However, CCS axons contacted apical branches more frequently in postsynaptic CPn cells than in CCS cells (Figs. 6*B*, 9*A*,*B*). The apical contact ratio (contacts on apical branches/total contacts) was lower in CCS cells than in CPn cells ($p < 0.05$) (Table 3).

To test whether unitary currents were correlated with the morphological distribution of contacts in the postsynaptic cells, we compared mean EPSC amplitudes with the number and position of contacts (Fig. 6*B*). EPSCs were detected even in the case of a single bouton located 220 μm from the soma (4.5 pA) (Fig. 6*B*). EPSC amplitudes per contact (see below) did not correlate well with the mean distance of contacts from the soma (c.c., 0.18, $p = 0.56$ in CCS to CCS pairs; c.c., −0.57, $p = 0.2$ in CCS to CPn pairs). EPSC amplitudes were better correlated with the number of contact sites rather than their spatial distribution (Figs. 6*B*, 7*A*). Additionally, this correlation was stronger in CCS to CCS pairs than in CCS to CPn pairs (c.c., 0.83, $p < 0.01$ in the former; c.c., 0.35, $p = 0.46$ in the latter). As expected, the EPSC CV was inversely correlated with the number of contact sites (Fig. 7*B*). These data suggest that the contact number reflects the number of synaptic release sites to some extent. When comparing between cell classes, significantly fewer contact sites were observed in CCS cells than were made onto CPn cells ($p = 0.01$) (Table 3). In the pairs for which both presynaptic and postsynaptic cells were reconstructed, mean somatic EPSC amplitudes were similar between CCS and CPn cells ($p = 0.91$) (Table 3). The EPSC amplitude divided by the number of contacts tended to be larger in CCS cells than CPn cells ($p = 0.06$) (Table 3), suggesting that the efficacy of individual synaptic release sites may be stronger in CCS to CCS cell pairs.

Contact formation probability between nearby neurites

Given the data above, we hypothesized that CCS and CPn cells show specificity in synapse formation onto postsynaptic den-

drites. To investigate whether CCS cells show preferences in postsynaptic targets, we compared the number of contacts generated by presynaptic axons onto postsynaptic dendrites with the total number of approaches (potential contact sites) in CCS to CCS or CCS to CPn pairs. First, we confirmed that contacts were never observed in pairs in which EPSCs were not detected (Fig. 9*B*). Two situations could explain this lack of connectivity: (1) if presynaptic axons do not come within range of the second neuron, synaptic formation would be impossible; or (2) presynaptic axons may approach the postsynaptic dendrites (within distances potential for synapse formation) but avoid making synaptic contacts (Fig. 8, inset). To discriminate between these two possibilities, we mapped the dendrites of potential postsynaptic neurons and identified all points (approach points) where the axons of the other recorded neuron approached within 2.5 μm from the dendritic center (Fig. 8). A distance of 2.5 μm was selected, because the average spine length varies from 1.8 to 2.6 μm (Stepanyants et al., 2002). Approach points included contact sites.

In nonreciprocally connected CCS–CCS pairs, the neuron with no observable EPSC had fewer approach points onto its basal dendrites than did the neuron with detectable EPSCs. The mean number of approach points in the nonsynaptically and synaptically connected neurons, respectively, was 7.2 ± 6.7 ($n = 6$) and 11.1 ± 5 ($n = 13$; $p = 0.1$) (Fig. 9*B*). In the CCS–CPn pairs, neurons with no EPSC detected had approximately half the number of approach points (mean, 7 ± 6.4; $n = 7$) onto their basal dendrites as did neurons with synaptic responses (mean, 14.6 ± 6.7; $n = 7$; $p = 0.05$). In the apical branches of CCS–CCS pairs, the number of approach points in neurons without postsynaptic EPSCs (1 ± 1.6) was approximately one-third of those in neurons with observable EPSCs (3.4 ± 2.6; $p = 0.05$) (Fig. 9*C*). Similarly, in CCS–CPn pairs, the number of apical approaches in nonresponding neurons (1.3 ± 1.8) was one-third of those in synaptically responsive neurons (4.7 ± 4.6; $p = 0.08$). These data demonstrate that opportunities for synaptic connections onto nontargeted neurons exist as evidenced by approach points onto both apical and basal dendrites.

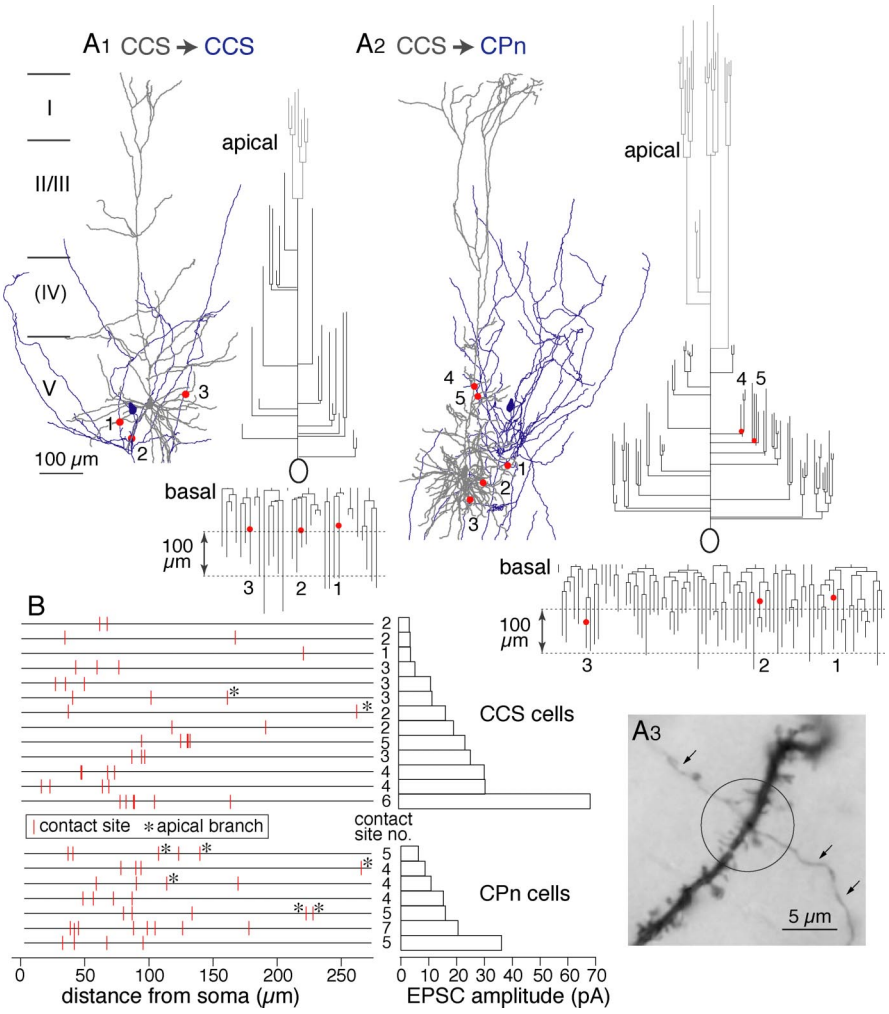

Figure 6. Contact sites between presynaptic axons and postsynaptic dendrites. ***A***, Examples of dendritic contact sites in a CCS to CCS connection (***A1***; 1–3) and a CCS to CPn connection (***A2***; 1–5). Dendrites are shown in gray, and axons are shown in blue. Contact sites (red circles) are shown on the dendrograms of the apical and basal dendrites. Apical tufts are shown in light gray. ***A3***, Photograph of a contact site between axon and dendrite in a CCS to CCS pair. The presynaptic axon is marked by arrows. ***B***, Plot of the distribution of contact sites along the dendrites of 13 CCS and 7 CPn cells (left) and the corresponding EPSC amplitude (right). Contacts on apical branches are marked by asterisks.

Table 3. Morphological contact sites and EPSC characteristics in the reconstructed pairs

	CCS ($n = 13$)	CPn ($n = 7$)
Contact sites on dendrites		
Contact site number	3.1 ± 1.4	4.9 ± 1.1*
Distance from somatic origin (μm)	90.9 ± 55.2	97.8 ± 57.8
Dendrite order	4.3 ± 1.9	4.3 ± 2.9
Apical contact ratio (contacts on apical branches/total contacts)	0.06 ± 0.16	0.19 ± 0.18*
Unitary EPSC amplitude (pA)	20.2 ± 17.9	16.6 ± 10.1
Unitary EPSC amplitude/contact site number (pA)	6.0 ± 3.2	3.4 ± 1.8

Data are means ± SD. *n*, Number of cells. *$p < 0.05$

We next compared the dendritic and spatial distribution patterns between approaches and contacts. The dendritic distribution patterns were similar between contacts and all approaches in the basal dendrites of connected pairs from CCS to CCS (Fig. 9*A1*, Table 4) (Kolmogorov–Smirnov test; $p = 0.59$ in basal dendrites) or CCS to CPn cells (Fig. 9*A2*, Table 4) ($p = 0.56$ in basal dendrites). The vertical spatial distributions of contact sites and approaches were similar in CCS to CPn pairs (Table 4) ($p = 0.34$). In CCS to CCS pairs, however, contact sites were more skewed toward the white matter side than approaches (Table 4) ($p < 0.05$), suggesting spatial selectivity during contact formation.

To estimate the probability of contact formation on nearby neurites, we compared the ratio of contacts to approaches (contact ratio) in basal dendrites and apical branches (Fig. 9*B*). CCS to

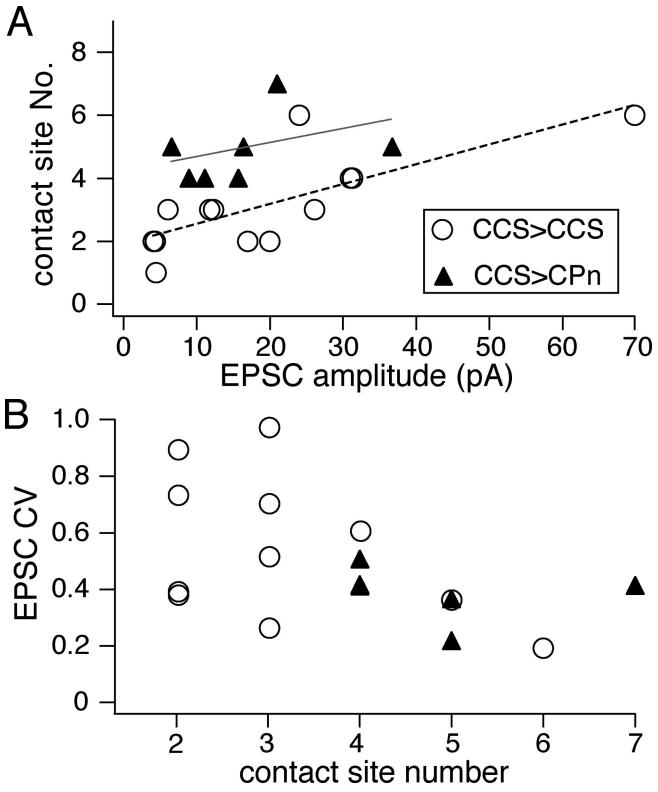

Figure 7. Relationship of contact site number and EPSC characteristics. ***A***, Relationship of contact site numbers with the corresponding EPSC amplitudes. The correlation in CCS to CCS pairs (linear fitting line in red) was stronger than that in CCS to CPn pairs (linear fitting line in gray). ***B***, Relationship of CV of EPSC amplitudes with the corresponding number of morphological contact sites, which were inversely correlated (c.c., -0.51; $p < 0.05$).

CCS pairs significantly favored synapse generation onto basal dendrites, with the contact ratio of the basal dendrites being 0.28 ± 0.14 ($n = 13$), compared with a contact ratio of only 0.09 ± 0.28 ($p < 0.01$) in apical branches. Conversely, CCS to CPn pairs showed greater balance in synapse formation onto basal and apical dendrites, with the contact ratio being 0.31 ± 0.14 ($n = 7$) in the basal dendrites and 0.24 ± 0.36 ($p = 0.13$) in the apical branches. These data suggest that the location of synapse formation between presynaptic CCS cells and nearby pyramidal neurons is target specific, and that synapses onto basal dendrites are favored when establishing contacts onto other CCS cells, although synapse formation onto CPn cells occurs on both basal and apical branches.

Discussion

Synaptic connection selectivity between pyramidal cell subtypes

Pyramidal cells are functionally connected with each other by local collaterals (Thomson and Deuchars, 1994; Markram et al., 1997; Mercer et al., 2005), and pyramidal cells in different layers are selectively connected (Thomson and Bannister, 2003; Feldmeyer et al., 2005). Pyramidal cells in the same layer appear to be connected in nonrandom ways (Markram et al., 1997; Song et al., 2005). Although subtypes of pyramidal neurons show differential patterns in their axonal projections to subcortical structures (Jones, 1984), it remains to be investigated how selective and precise the recurrent connections are among pyramidal cell subtypes within the neocortex. In this study, for the first time, we investigated the synaptic connection patterns of corticostriatal subtypes identified by both their axonal projection pattern and their dendritic structure. Our data demonstrate that there is significant specificity in the connectivity of cortical pyramidal neurons.

Layer V pyramidal neurons with distinct tuft structures were differentially connected in a direction-selective way (Fig. 10): CCS cells formed synapses onto CPn cells, but there were few connections from CPn to CCS cells, although the axons of CPn cells frequently approached CCS dendrites at distances close enough to facilitate synapse formation. In addition to direction selectivity, CCS cells preferentially innervate the basal dendrites of other CCS cells but show more balanced innervation of the basal and apical dendrites of CPn cells.

In one case, a single bouton, further than 200 μm, was found to generate a unitary CCS to CCS EPSC at the soma. More generally, EPSC amplitudes induced in CCS cells by other CCS cells were correlated with the number of presynaptic boutons to some extent. This suggests that the number of contact sites in CCS to CCS pairs is correlated with the functional synaptic number (Markram et al., 1997; Kalisman et al., 2005). Different ratios of the EPSC amplitude to contact number were found between the two connections, although not significant. There may be target-specific differences in synaptic efficacy or synaptic integration in these two cell types (Feldmeyer and Sakmann, 2000).

In the case of CCS to CCS connections, slender cells tended to form synaptic connections with other slender cells, although tufted cells preferred similarly tufted neurons. These correlations likely result, in part, because CCS cells in the same sublaminar area of layer V tended to have similar dendritic morphologies (Fig. 10), and most synaptically connected neurons were found within 100 μm of each other. These findings suggest that CCS pyramidal cells with similar dendritic morphologies (and therefore to some extent similar afferent input) may be locally clustered within layer V and show preferential synaptic connectivity. This may reflect vertical aggregates of neurons with a similar target during cortical formation (Vercelli et al., 2004).

Corticostriatal cell heterogeneity and their intracortical connections

Pyramidal cells projecting to the striatum are considered to be functionally heterogeneous (Wilson, 2004). To date, two subtypes of corticostriatal cells have been identified. The first identified subtype, demonstrated in both primates (Jones et al., 1977) and rats (Wilson, 1987), are corticostriatal neurons that do not project to the brainstem but that innervate the contralateral striatum. This innervation pattern was later confirmed using intracellular staining of axons (Cowan and Wilson, 1994; Lévesque et al., 1996a,b). A second subtype of CCS cell identified in rats projects to the brainstem (Donoghue and Kitai, 1981; Cowan and Wilson, 1994; Lévesque et al., 1996a). Although it remains to be investigated how often collaterals are issued from axons descending to the brainstem in the primate (Bauswein et al., 1989), in the rat frontal cortex, brainstem-projecting layer V neurons also frequently innervate the ipsilateral striatum (Lévesque et al., 1996a; Lévesque and Parent, 1998). In this study, we confirmed that CCS and CPn cells are mutually exclusive groups using double-fluorescence markers. Apical dendritic tufts are different in size among pyramidal cell subtypes (Hallman et al., 1988; Hübener et al., 1990; Kasper et al., 1994; Gao and Zheng, 2004). In addition to their striking differences in axonal projection, we found significant morphological differences in their apical tuft structures (Fig. 10). Furthermore, CCS cells were heterogeneous with regard to their tuft branching pattern, showing significant correlation be-

tween somatic depth and the degree of dendritic arborization in layer I.

Because CCS and CPn cells are differentiated in their dendritic structures, synaptic connectivity, and extracortical projection sites, it is possible that they receive distinct types of inputs within the frontal cortex. Information transfer in the frontal cortical circuit is a crucial point for the forebrain neural loop through the cortex, basal ganglia, and thalamus, involved in the context-dependent release of various motor and cognitive circuits (Graybiel et al., 1994; Hikosaka et al., 2002). Therefore, it is important to know how these two types of corticostriatal cells are innervated by afferent fibers from the mediodorsal and parafascicular thalamic nuclei, areas that receive GABAergic inhibition from the basal ganglia (Kuroda et al., 1998; Cebrián et al., 2005). Thalamic fibers distribute in layer I and the deep part of layer II/III (Deschênes et al., 1996; Marini et al., 1996; Jones, 2001). Both CCS and CPn cells have apical branches in the deeper layer II/III, whereas the apical tuft expansions within layer I are distinct between CCS and CPn cells and heterogeneous among CCS cells. It remains to be investigated which subtypes of layer V corticostriatal cells receive thalamic inputs directly at the layer I tufts at or at deeper layer II/III.

Thalamic afferents innervate layer II/III pyramidal cells in addition to layer V cells (Kuroda et al., 1998). Layer II/III pyramidal cells preferentially innervate thick tufted layer V pyramidal cells rather than slender layer V pyramidal cells (Thomson and Bannister, 1998; Thomson and Morris, 2002). Therefore, layer II/III pyramidal cells with direct inputs from the thalamic nuclei may preferentially innervate CPn cells over CCS cells. Additional investigations elucidating the specifics of intracortical wiring between specific classes of cortical neurons will be needed to understand the influence of cortical circuits on striatal output.

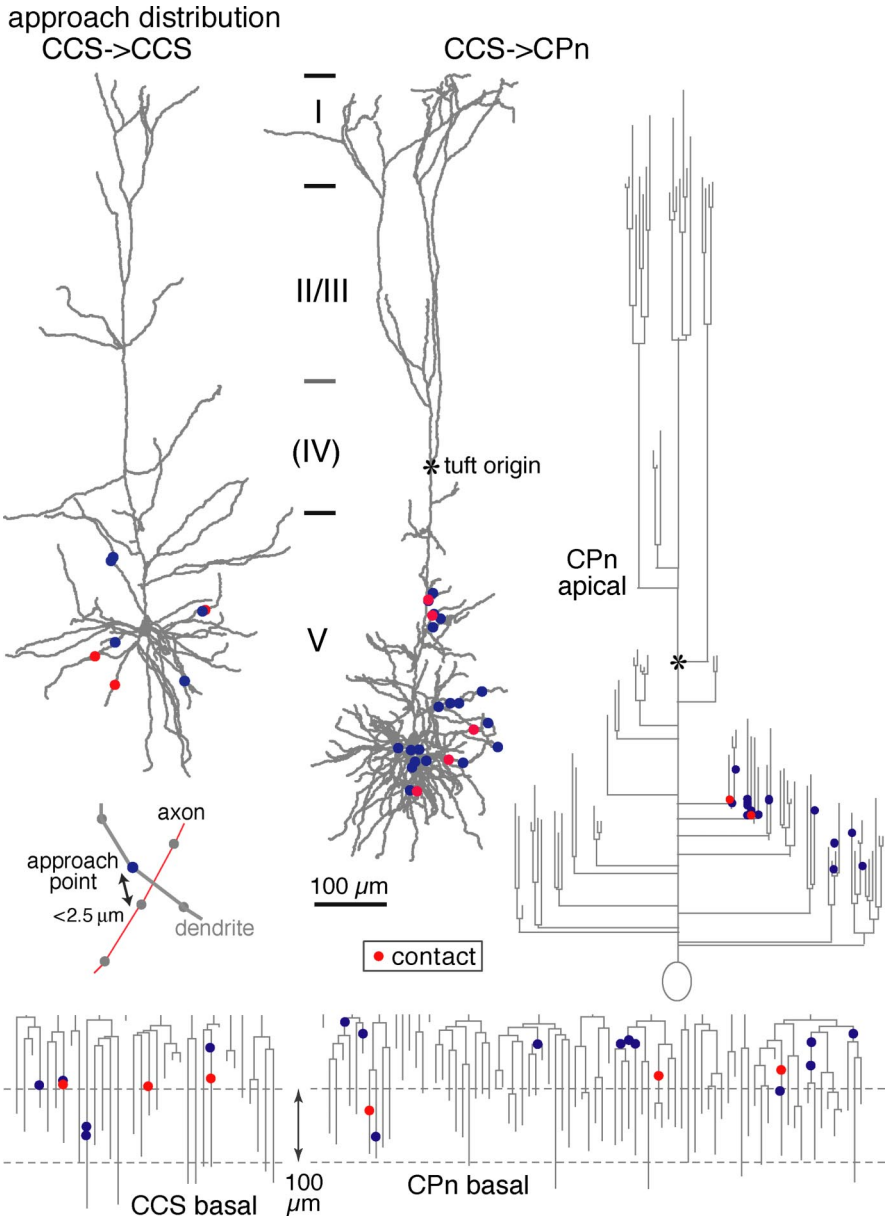

Figure 8. Distributions of approach points along reconstructed dendrites and dendrograms of example postsynaptic neurons (basal dendrites of a CCS cell, and basal and apical dendrites of a CPn cell). Contact sites are shown in red, and noncontact approach points are shown in blue. Inset, Example of an approach point (blue circle) of an axon (red line) to a dendrite (gray line). Reconstructed axons and dendrites were composed of serial points (circles) with intervals shorter than 1.5 μm. Approach points were defined as dendritic sites where axons passed within 2.5 μm.

Functional differentiation of corticostriatal pathways

In this study, we found that differential axonal projections and apical tuft structures segregate corticostriatal cells into two types, with CCS cells further differentiated according to their depth-dependent differences in dendritic morphology. This suggests that corticostriatal neurons are heterogeneous according to their extracortical target and the laminar location. Similarly, in the striatum, projection cells are heterogeneous from two independent points of view: the extrastriatal target and intrastriatal location.

In terms of extrastriatal targets, they are divided mainly into two groups (Gerfen and Young, 1988; Kawaguchi et al., 1990; Parent et al., 1995). These two types are considered to affect basal ganglia outputs in opposite ways (Albin et al., 1989; Alexander and Crutcher, 1990). One group exclusively projects to the external pallidal segment (GPe-exclusive cells; indirect pathway), whereas another group, while sending axon collaterals to the external pallidal segment, directly projects to output structures in the basal ganglia (direct pathway cells) (Kawaguchi et al., 1990; Lévesque and Parent, 2005). Direct pathway cells are considered to promote desired movements, and GPe-exclusive cells are considered to inhibit unwanted movement (Albin et al., 1989; DeLong, 1990; Lei et al., 2004). Recently, it has been revealed that two types of corticostriatal cells differentially innervate one of the above two striatal output cells (Reiner et al., 2003; Lei et al., 2004). In light of these data, it is likely that CPn cells preferentially innervate GPe-exclusive cells while CCS cells innervate direct pathway cells. Therefore, activity in CPn cells may promote dis-

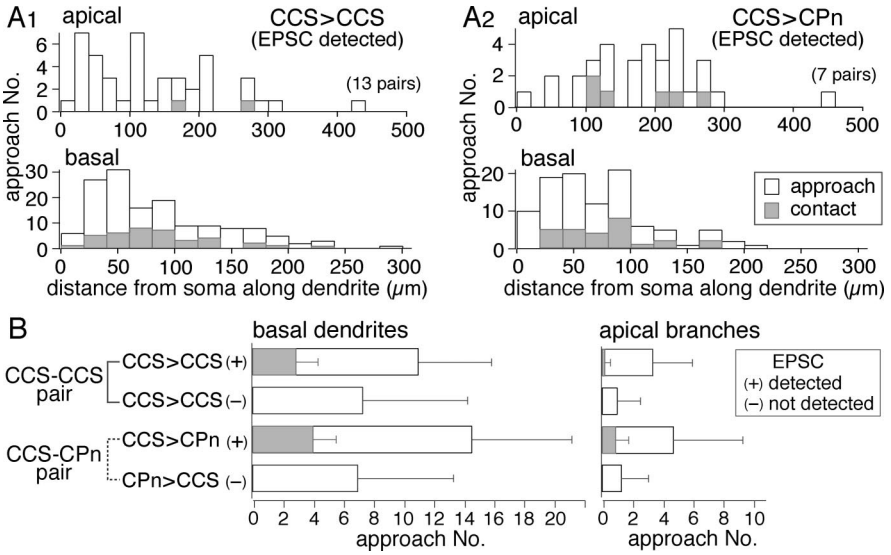

Figure 9. Frequency of axonal contacts onto nearby postsynaptic dendrites. ***A1***, ***A2***, Dendritic distance distributions of total approaches and contacts along dendrites from soma in connected CCS to CCS (***A1***; from 13 cells) and CCS to CPn (***A2***; from 7 cells) pairs; those at the top are in apical branches, and those at the bottom are in basal dendrites. The distribution patterns were similar between approaches and contacts in basal dendrites of connected pairs. Apical branch contacts were more frequent in connected CCS to CPn than in CCS to CCS pairs. ***B***, Mean number of approach points and contact sites in CCS–CCS and CCS–CPn pairs. Data are shown separately for basal and apical branches. Pairs with unitary EPSCs (marked by +) always showed contact sites. Unconnected pairs had no contact sites and fewer approaches. Note that contact site ratios in basal dendrites of both types and apical dendrites of CPn cells were similar (0.2–0.3), but those in apical dendrites of CCS cells were much lower. Data are means ± SD.

Table 4. Dendritic and spatial distributions of contact sites and approach points

	CCS		CPn	
	($n = 13$ cells)		($n = 7$ cells)	
	Contacts	Approaches	Contacts	Approaches
Dendritic distribution (distance from somatic origin, μm)				
Apical branches	161, 262.3 ($n = 2$)	133.5 ± 93.9 ($n = 44$)	179.5 ± 68.4 ($n = 6$)	191.8 ± 75.3 ($n = 33$)
Basal dendrites	84.5 ± 47.4 ($n = 38$)	85.0 ± 56.1 ($n = 144$)	80.7 ± 39 ($n = 28$)	71.3 ± 45.3 ($n = 102$)
Spatial distribution				
Vertical projection (μm) (position from somatic centroid[a])	−26.4 ± 66.1 ($n = 40$)	−6.1 ± 82.1* ($n = 188$)	9.6 ± 74.7 ($n = 34$)	17.4 ± 72.5 ($n = 135$)
Tangential projection (μm) (position from somatic centroid[b])	4.2 ± 48.8	0.65 ± 49.5	−5.8 ± 45.6	−11.6 ± 46.8

Data are means ± SD. *n*, Number of cells, total approaches, or contact sites. Approach points include contact sites. *$p < 0.05$.

[a]Pia side, positive.

[b]Medial side, positive.

crete motor outputs to the brainstem or spinal cord through the pyramidal tract but suppress unnecessary outputs by excitation of GPe-exclusive cells in the striatum. Interestingly, CPn cells that synapse on the indirect-pathway striatal neurons likely receive more excitatory synaptic input because of their enlarged dendritic trees in layer I relative to CCS cells. In addition, CPn cells are excited by CCS cells while not providing significant feedback excitation, and only CCS cells project to the other hemisphere. In view of these connection patterns, CCS cells seem to regulate the activity balance between the direct and indirect pathways or also between both sides of basal ganglia.

The intrastriatal locations divided striatal projection cells into two groups, independent of the above extrastriatal projections ones. These two groups of neurons are spatially compartmentalized within the striatum, with one group forming irregularly shaped patches within a surrounding matrix composed of neurons of the other class (Gerfen, 1984, 1992; Kawaguchi et al., 1989). Striatal neurons in each compartment receive distinct cortical afferents from specific cortical regions and laminas. Deep layer V corticostriatal neurons project principally to patch neurons, whereas superficial layer V corticostriatal neurons project principally to neurons in the matrix (Gerfen, 1989). The sublaminar differentiation of layer V CCS cells may be related to their relative contribution to patch and matrix innervation. Our data suggest that the different pathways within the basal ganglia are already differentiated within the intracortical circuits. The heterogeneity in dendritic morphology, sublaminar position, and synaptic formation in CCS and CPn cells may correspond to the striatal cell differentiation and compartmentalization.

References

Albin RL, Young AB, Penney JB (1989) The functional anatomy of basal ganglia disorders. Trends Neurosci 12:366–375.

Alexander GE, Crutcher MD (1990) Functional architecture of basal ganglia circuits: neural substrates of parallel processing. Trends Neurosci 13:266–271.

Anderson J, Lampl I, Reichova I, Carandini M, Ferster D (2000) Stimulus dependence of two-state fluctuations of membrane potential in cat visual cortex. Nat Neurosci 3:617–621.

Bauswein E, Fromm C, Preuss A (1989) Corticostriatal cells in comparison with pyramidal tract neurons: contrasting properties in the behaving monkey. Brain Res 493:198–203.

Christophe E, Doerflinger N, Lavery DJ, Molnar Z, Charpak S, Audinat E (2005) Two populations of layer V pyramidal cells of the mouse neocortex: development and sensitivity to anesthetics. J Neurophysiol 94:3357–3367.

Cebrián C, Parent A, Prensa L (2005) Patterns of axonal branching of neurons of the substantia nigra pars reticulata and pars lateralis in the rat. J Comp Neurol 492:349–369.

Cowan RL, Wilson CJ (1994) Spontaneous firing patterns and axonal projections of single corticostriatal neurons in the rat medial agranular cortex. J Neurophysiol 71:17–32.

DeLong MR (1990) Primate models of movement disorders of basal ganglia origin. Trends Neurosci 13:281–285.

Deschênes M, Bourassa J, Doan VD, Parent A (1996) A single-cell study of the axonal projections arising from the posterior intralaminar thalamic nuclei in the rat. Eur J Neurosci 8:329–343.

Donoghue JP, Kitai ST (1981) A collateral pathway to the neostriatum from corticofugal neurons of the rat sensory-motor cortex: an intracellular HRP study. J Comp Neurol 201:1–13.

Feldmeyer D, Sakmann B (2000) Synaptic efficacy and reliability of excitatory connections between the principal neurones of the input (layer 4) and output layer (layer 5) of the neocortex. J Physiol (Lond) 525:31–39.

Feldmeyer D, Egger V, Lübke J, Sakmann B (1999) Reliable synaptic connections between pairs of excitatory layer 4 neurones within a single "barrel" of developing rat somatosensory cortex. J Physiol (Lond) 521:169–190.

Feldmeyer D, Roth A, Sakmann B (2005) Monosynaptic connections between pairs of spiny stellate cells in layer 4 and pyramidal cells in layer 5A indicate that lemniscal and paralemniscal afferent pathways converge in the infragranular somatosensory cortex. J Neurosci 25:3423–3431.

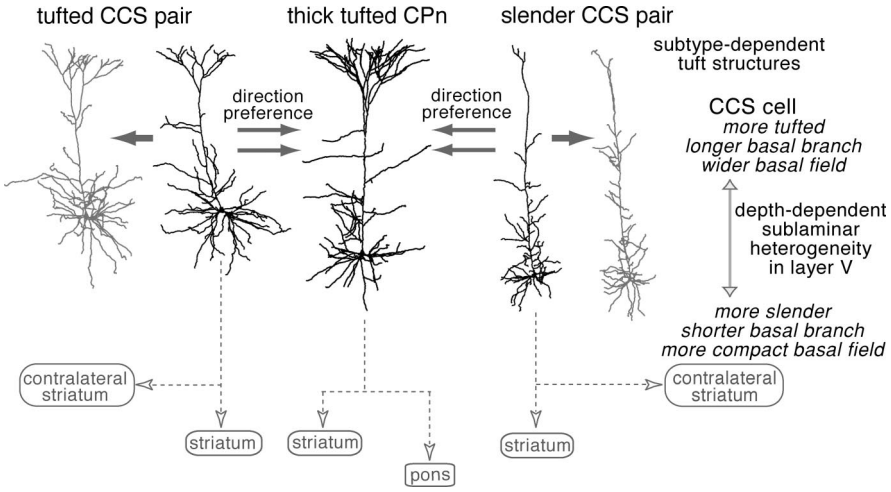

Figure 10. Innervation hierarchy and morphological pairing in synaptic connections between CCS and CPn cells. CCS cells were connected with each other and also with CPn cells, but connections from CPn to CCS cells were rarely found. Innervated domains were both basal and apical branches in the pairs from CCS to CPn cells but mostly basal dendrites in those between CCS cells. CCS cells were often connected with other CCS cells with similar dendritic patterns. CCS cells were heterogeneous in apical tuft and basal structures, which were dependent on the somatic depth from pia.

Gabbott PLA, Warner TA, Jays PR, Salway P, Busby SJ (2005) Prefrontal cortex in the rat: projections to subcortical autonomic, motor, and limbic centers. J Comp Neurol 492:145–177.

Gao WJ, Zheng ZH (2004) Target-specific differences in somatodendritic morphology of layer V pyramidal neurons in rat motor cortex. J Comp Neurol 476:174–185.

Gao W-J, Krimer LS, Goldman-Rakic PS (2001) Presynaptic regulation of recurrent excitation by D1 receptors in prefrontal circuits. Proc Natl Acad Sci USA 98:295–300.

Gerfen CR (1984) The neostriatal mosaic: compartmentalization of corticostriatal input and striatonigral output systems. Nature 311:461–464.

Gerfen CR (1989) The neostriatal mosaic: striatal patch-matrix organization is related to cortical lamination. Science 246:385–388.

Gerfen CR (1992) The neostriatal mosaic: multiple levels of compartmental organization in the basal ganglia. Annu Rev Neurosci 15:285–320.

Gerfen CR, Young WS (1988) Distribution of striatonigral and striatopallidal peptidergic neurons in both patch and matrix compartments: an in situ hybridization histochemistry and fluorescent retrograde tracing study. Brain Res 460:161–167.

Graybiel AM, Aosaki T, Flaherty AW, Kimura M (1994) The basal ganglia and adaptive motor control. Science 265:1826–1831.

Hallman LE, Schofield BR, Lin CS (1988) Dendritic morphology and axon collaterals of corticotectal, corticopontine, and callosal neurons in layer V of primary visual cortex of the hooded rat. J Comp Neurol 272:149–160.

Hefti BJ, Smith PH (2000) Anatomy, physiology, and synaptic responses of rat layer V auditory cortical cells and effects of intracellular $GABA_A$ blockade. J Neurophysiol 83:2626–2638.

Hikosaka O, Nakamura K, Sakai K, Nakahara H (2002) Central mechanisms of motor skill learning. Curr Opin Neurobiol 12:217–222.

Holmgren C, Harkany T, Svennenfors B, Zilberter Y (2003) Pyramidal cell communication within local networks in layer 2/3 of rat neocortex. J Physiol (Lond) 551:139–153.

Hübener M, Schwarz C, Bolz J (1990) Morphological types of projection neurons in layer 5 of cat visual cortex. J Comp Neurol 301:655–674.

Jones EG (1984) Laminar distribution of output cells. In: Cerebral cortex, Vol 1, Cellular components of the cerebral cortex (Peters A, Jones EG, eds), pp 521–553. New York: Plenum.

Jones EG (2001) The thalamic matrix and thalamocortical synchrony. Trends Neurosci 24:595–601.

Jones EG, Coulter JD, Burton H, Porter R (1977) Cells of origin and terminal distribution of corticostriatal fibers arising in the sensory-motor cortex of monkeys. J Comp Neurol 173:53–80.

Kalisman N, Silberberg G, Markram H (2005) The neocortical microcircuit as a tabula rasa. Proc Natl Acad Sci USA 102:880–885.

Karube F, Kubota Y, Kawaguchi Y (2004) Axon branching and synaptic bouton phenotypes in GABAergic nonpyramidal cell subtypes. J Neurosci 24:2853–2865.

Kasper EM, Larkman AU, Lübke J, Blakemore C (1994) Pyramidal neurons in layer 5 of the rat visual cortex. I. Correlation among cell morphology, intrinsic electrophysiological properties, and axon targets. J Comp Neurol 339:459–474.

Kawaguchi Y (1992) Receptor subtypes involved in callosally-induced postsynaptic potentials in rat frontal agranular cortex in vitro. Exp Brain Res 88:33–40.

Kawaguchi Y, Wilson CJ, Emson PC (1989) Intracellular recording of identified neostriatal patch and matrix spiny cells in a slice preparation preserving cortical inputs. J Neurophysiol 62:1052–1068.

Kawaguchi Y, Wilson CJ, Emson PC (1990) Projection subtypes of rat neostriatal matrix cells revealed by intracellular injection of biocytin. J Neurosci 10:3421–3438.

Kuroda M, Yokofujita J, Murakami K (1998) An ultrastructural study of the neural circuit between the prefrontal cortex and the mediodorsal nucleus of the thalamus. Prog Neurobiol 54:417–458.

Lei W, Jiao Y, Del Mar N, Reiner A (2004) Evidence for differential cortical input to direct pathway versus indirect pathway striatal projection neurons in rats. J Neurosci 24:8289–8299.

Lévesque M, Parent A (1998) Axonal arborization of corticostriatal and corticothalamic fibers arising from prelimbic cortex in the rat. Cereb Cortex 8:602–613.

Lévesque M, Parent A (2005) The striatofugal fiber system in primates: a reevaluation of its organization based on single-axon tracing studies. Proc Natl Acad Sci USA 102:11888–11893.

Lévesque M, Charara A, Gagnon S, Parent A, Deschênes M (1996a) Corticostriatal projections from layer V cells in rat are collaterals of long-range corticofugal axons. Brain Res 709:311–315.

Lévesque M, Gagnon S, Parent A, Deschênes M (1996b) Axonal arborizations of corticostriatal and corticothalamic fibers arising from the second somatosensory area in the rat. Cereb Cortex 6:759–770.

Marini G, Pianca L, Tredici G (1996) Thalamocortical projection from the parafascicular nucleus to layer V pyramidal cells in frontal and cingulate areas of the rat. Neurosci Lett 203:81–84.

Markram H (1997) A network of tufted layer 5 pyramidal neurons. Cereb Cortex 7:523–533.

Markram H, Lübke J, Frotscher M, Roth A, Sakmann B (1997) Physiology and anatomy of synaptic connections between thick tufted pyramidal neurones in the developing rat neocortex. J Physiol (Lond) 500:409–440.

Mason A, Larkman A (1990) Correlations between morphology and electrophysiology of pyramidal neurons in slices of rat visual cortex. II. Electrophysiology. J Neurosci 10:1415–1428.

Mercer A, West DC, Morris OT, Kirchhecker S, Kerkhoff JE, Thomson AM (2005) Excitatory connections made by presynaptic cortico-cortical pyramidal cells in layer 6 of the neocortex. Cereb Cortex 15:1485–1496.

Metherate R, Ashe JH (1993) Ionic flux contributions to neocortical slow waves and nucleus basalis-mediated activation: whole-cell recordings *in vivo*. J Neurosci 13:5312–5323.

Parent A, Charara A, Pinault D (1995) Single striatofugal axons arborizing in both pallidal segments and in the substantia nigra in primates. Brain Res 698:280–284.

Reiner A, Jiao Y, Del Mar N, Laverghetta AV, Lei WL (2003) Differential morphology of pyramidal tract-type and intratelencephalically projecting-type corticostriatal neurons and their intrastriatal terminals in rats. J Comp Neurol 457:420–440.

Sanchez-Vives MV, McCormick DA (2000) Cellular and network mechanisms of rhythmic recurrent activity in neocortex. Nat Neurosci 3:1027–1034.

Song S, Sjöström PJ, Reigl M, Nelson S, Chklovskii DB (2005) Highly non-

random features of synaptic connectivity in local cortical circuits. PLoS Biol 3:507–519.

Stepanyants A, Hof PR, Chklovskii DB (2002) Geometry and structural plasticity of synaptic connectivity. Neuron 34:275–288.

Steriade M, Nunez A, Amzica F (1993) Intracellular analysis of relations between the slow (<1 Hz) neocortical oscillation and other sleep rhythms of the electroencephalogram. J Neurosci 13:3266–3283.

Stern EA, Kincaid AE, Wilson CJ (1997) Spontaneous subthreshold membrane potential fluctuations and action potential variability of rat corticostriatal and striatal neurons in vivo. J. Neurophysiol 77:1697–1715.

Stern EA, Jaeger D, Wilson CJ (1998) Membrane potential synchrony of simultaneously recorded striatal spiny neurons in vivo. Nature 394:475–478.

Thomson AM, Bannister AP (1998) Postsynaptic pyramidal target selection by descending layer III pyramidal axons: dual intracellular recordings and biocytin filling in slices of rat neocortex. Neuroscience 84:669–683.

Thomson AM, Bannister AP (2003) Interlaminar connections in the neocortex. Cereb Cortex 13:5–14.

Thomson AM, Deuchars J (1994) Temporal and spatial properties of local circuits in neocortex. Trends Neurosci 17:119–126.

Thomson AM, Deuchars J (1997) Synaptic interactions in neocortical local circuits: dual intracellular recordings in vitro. Cereb Cortex 7:510–522.

Thomson AM, Morris OT (2002) Selectivity in the inter-laminar connections made by neocortical neurones. J Neurocytol 31:239–246.

Vercelli AE, Garbossa D, Curtetti R, Innocenti GM (2004) Somatodendritic minicolumns of output neurons in the rat visual cortex. Eur J Neurosci 20:495–502.

Wang XJ (2001) Synaptic reverberation underlying mnemonic persistent activity. Trends Neurosci 24:455–463.

Wang Z, McCormick DA (1993) Control of firing mode of corticotectal and corticopontine layer V burst-generating neurons by norepinephrine, acetylcholine, and 1*S*,3*R*-ACPD. J Neurosci 13:2199–2216.

Wilson CJ (1987) Morphology and synaptic connections of crossed corticostriatal neurons in the rat. J Comp Neurol 263:567–580.

Wilson CJ (2004) Basal ganglia. In: The synaptic organization of the brain, Ed 5 (Shepherd GM, ed), pp 361–413. New York: Oxford UP.

Wilson CJ, Groves PM (1981) Spontaneous firing patterns of identified spiny neurons in the rat neostriatum. Brain Res 220:67–80.

Wilson CJ, Kawaguchi Y (1996) The origins of two-state spontaneous membrane potential fluctuations of neostriatal spiny neurons. J Neurosci 16: 2397–2410.